Scientific Reports

https://doi.org/10.1038/s41598-026-36212-y

Article in Press

Epidemic spread with asymptomatic infectious period in contact adaptive networks

Received: 13 February 2025

Accepted: 9 January 2026

Published online: 23 January 2026

Cite this article as: Chai W.K. & Karaliopoulos M. Epidemic spread with asymptomatic infectious period in contact adaptive networks. *Sci Rep* (2026). https://doi.org/10.1038/s41598-026-36212-y

Wei Koong Chai & Merkourios Karaliopoulos

Epidemic Spread with Asymptomatic Infectious Period in Contact Adaptive Networks

Wei Koong Chai[1,*] **and Merkourios Karaliopoulos**[2]

[1]School of Computing & Engineering, Bournemouth University, UK
[2]Information Technologies Institute, Centre for Research and Technology, Thessaloniki, Greece
[*]wchai@bournemouth.ac.uk

ABSTRACT

We model an epidemic spread process involving nodes that (a) experience non-trivial asymptomatic infectious periods and (b) adapt by avoiding contacts with symptomatic infectious nodes. These modeling choices reflect ample evidence that infectious individuals are often mistakenly perceived as safe contacts due to lack of symptoms and that individuals adapt to an epidemic by avoiding contacts deemed to be of risk. We capture these choices in the SI^aI^sS (Susceptible-Asymptomatic Infected-Symptomatic Infected-Susceptible) model, where we explicitly distinguish between asymptomatic and symptomatic infectious individuals. We adopt an individual-based mean-field epidemic modeling approach and formulate the system of differential equations via continuous-time Markov chain analysis. We first consider non-adaptive homogeneous and heterogeneous mixing scenarios over arbitrary static contact networks. We derive the expression for the basic reproduction number, $\mathscr{R}_0$, and establish that under otherwise similar conditions the individual infection probabilities at the metastable state of SI^aI^sS dominate those in the conventional SIS model. Then, we focus on a contact-adaptive setting, where nodes avoid interactions with known infectious neighbors or reconnect with neighbors who have recovered, to study how the time-varying contact network, asymptomatic infections and their combinations affect the epidemic spread dynamics. Overall, asymptomatic infections restrict nodes' capacity to adapt (link breaking), resulting in higher link density and consequently higher epidemic prevalence. Besides, in their presence, the retarding effect of the link-breaking mechanism on epidemic prevalence is considerably mitigated. We numerically analyze how the effective link-breaking rate and the size of the asymptomatically infected population affect the link density and, ultimately, the epidemic prevalence. Furthermore, the epidemic threshold appears to scale inversely with the population of asymptomatic nodes, namely the epidemic starts to spread at lower infection rates when the number of asymptomatic infections is higher.

Introduction

After the recent COVID-19 pandemic outbreak, research effort is globally invested anew in understanding disease spreading phenomena. One particular aspect of these phenomena that has drawn much attention in literature relates to the role of *silent spreaders*[1]; namely, individuals who are infectious yet "unobservable" because they do not exhibit disease symptoms. When individuals exhibit infection symptoms, people in their social surroundings may intentionally avoid contacts with them. This way the corresponding links in their social contact network are broken and the disease spread is decelerated. On the contrary, infected individuals without symptoms are perceived as healthy and neither can they self-isolate voluntarily nor can others avoid contacts with them. Without proper contact adaptation amongst the population, these individuals may inadvertently trigger new infection chains. Silent spreaders are relevant not only for biological diseases but also for other spreading processes such as botnets, malware and ransomware attacks, where infected nodes lay dormant prior to attack and infected victims are often unaware of their infection[2–4]. The interplay between (1) the effect of silent spreaders and (2) the contact adaptation process that occurs as a result of individual responses to the epidemic spread is complex: the spreading process changes the contact network structure, which in turn changes the spreading process, realizing a non-trivial feedback loop and highlighting a continuous interaction between the two. The literature has promptly identified the importance of these two factors, yet their impact has been routinely studied in isolation.

With respect to silent spreaders, 5 extended the classic *SIR* epidemic model and proposed the *SAIR* model by introducing a new "Asymptomatic" state to study the emergence of drug resistance. This model has been more recently further investigated in 6 in the context of population migration across geographic regions. On the other hand, 7 proposed to split the "Infected" state in the *SIR* model into two sub-states (symptomatic and asymptomatic), introducing separate infection and recovery rates for each one. Recent work has also highlighted the importance of correctly recognizing and reacting to the infection risk. It is reported in 8 that (a) the spread of the epidemic is larger as the fraction of population not responding to the infection threat increases; and (b) the structure of the social contact network affects the peak of hospitalization: the higher its modularity

and heterogeneity, the lower the hospitalization peaks. In 9, the authors applied a modified *SIR* model accounting for a large population of asymptomatic nodes to the early COVID-19 infection data in northern Italy and highlighted that models disregarding asymptomatic population seriously underestimate important epidemic parameters such as its prevalence. This is corroborated in 10 working with COVID-19 data from two US cities. However, while coarse-grained aggregate data such as the number of infections and hospitalizations are more widely available, detailed node-level contact adaptation data is not easily obtained. In the absence of suitable behavioral data, 11 numerically explore the effect of risk misperception and find that even in the presence of behavioral change in human contacts, the asymptomatic population increases the epidemic prevalence.

Meanwhile, there is a body of work on epidemic spreading over time-varying network structures. At a first level, we can distinguish between two types of temporal networks: (1) non-adaptive time-varying networks that change independently of the epidemic process and (2) adaptive time-varying networks, whereby the existence of links depends on the state of the nodes. Reference 12 studied a variation of the *SIS* model[13] on a non-adaptive time-varying network, whose links are randomly activated/deleted, and questioned the value of basic reproduction number, $\mathscr{R}_0$, as predictor of long-term outcomes in dynamic networks. In 14, the authors compared time-varying contact networks, modeled after the fixed history of real human contacts, against static networks that aggregate contacts over time and fully connected networks. They found that removing temporal information leads to severe under- or over-estimation of outbreak characteristics and that long-term temporal structures are the most influential factors controlling the time to extinction and outbreak size. In 15, the researchers combine Monte Carlo simulations with mean-field theory to analyze the epidemic threshold. Their analysis incorporates network correlations (reflecting the persistence of social contacts) but ignores dynamic correlations (where being near infected nodes increases infection likelihood). They demonstrate that when the time scales of network dynamics and epidemic propagation are similar, the epidemic threshold depends explicitly on the recovery rate, as opposed to only the ratio of spreading rate over recovery rate. The latter is the case for annealed contact networks (network changes are much faster than the spread dynamics) and static contact networks (network changes are much slower than the spread dynamics).

At a second level, the adaptive time-varying networks can be further categorized into two main groups depending on how the network structure dynamics are modeled.

1. Under the *link rewiring* approach, a node may randomly switch a link to an existing neighbor with a link to another node with certain probability conditioned upon the states of the neighbor node[16–18]. Based on this approach, 16 found that the network structure exhibits assortative degree correlation and results in a highly connected susceptible cluster. The spreading process exhibits bistability and oscillations that are not evidenced in static contact networks.

2. Under the *link breaking/creating* approach, a node either breaks or creates a link with its neighbor node with certain probability depending on the state of the neighbor node[19,20]. In contrast with the link rewiring approach, a node does not necessarily connect to another node after breaking a link. For instance, 20 investigated different node response behaviors to epidemic and found that the relation between the epidemic threshold and the effective link-breaking rate could be linear or constant and in some cases, even unknown (*i.e.*, the metastable state is not found). This is the approach we adopt in our work.

The combined effect of asymptomatic individuals and the time-varying contact network on the epidemic spread has only recently gained research attention. Using agent-based simulations, 21 studied the phase transitions of epidemic spread caused by infectious individuals with pre-symptomatic, asymptomatic and symptomatic stages in small world networks that change under three schemes: (1) global social distancing with tunable probability of adherence, (2) probabilistic self-initiated social isolation and (3) reduction in viral shedding rate. The authors found that viral shedding rate is the most important driver in determining infection spreading. In 22, the authors employed activity-driven networks, whereby nodes and links are randomly activated, to study epidemic spreading with both asymptomatic and symptomatic populations. Finally, 23 investigated control measures for epidemic with asymptomatic carriers using a two-layer temporal network model. Whereas all these studies explicitly considered asymptomatic population and contact networks that change over time, the latter changes are routinely driven by tunable random processes rather than the state of linked nodes.

Contributions

Our work contributes to the long research thread on epidemic processes in three ways. *First*, we develop a novel epidemic model, SI^aI^sS, that jointly captures the role of asymptomatic infected individuals in the epidemic spread and the counter effect of changes in the individual contact networks in response to this spread. In our model, which inherits from the simple yet widely used *SIS* model, we explicitly distinguish the infected individuals into symptomatic (I^s) and asymptomatic (I^a) compartments and, thus, can more naturally relate link creation and breaking to the status of the epidemic. This marks a clear line of separation from the body of current literature, which rarely looks into the combined effect of the two factors and, when it does, the contact network changes are driven by random processes rather than being dependent on the nodes' state. We

Table 1. Key Mathematical Notations

Symbols	Descriptions
$A, A(t)$	Adjacency matrix representing the topology, time-dependent adjacency matrix
$\mathscr{V}, N$	The set and number of nodes (or vertices) in the network respectively
$\mathscr{E}, L$	The set and number of links (or edges) in the network respectively
β, γ	Infection and recovery rate respectively
σ	Symptom development rate (transition from Asymptomatic to Symptomatic)
ε	Proportion of infections that are asymptomatic
δ	Proportion of asymptomatic nodes that recover without developing symptoms
$s_n(t)$, $i_n^a(t)$, $i_n^s(t)$	Probability that node n lies in the healthy, asymptomatic infected and symptomatic infected state, respectively
ζ, ξ	Link breaking and link creation rate respectively
$\rho(t)$	Fraction of infected nodes in the network at time t
Q_n	Infinitesimal generator of node n's continuous Markov chain
$\mathscr{K}$	Next generation matrix
$\mathscr{R}_0$	Basic reproduction number
τ_c	Epidemic threshold
$\lambda_1(A)$	Largest eigenvalue of matrix A

adopt the individual-based mean-field approach[24], whereby input is the network topology and a continuous-time Markov chain models the coupling between the spreading process and the network evolution. The mean-field approximations reduce the overall analysis complexity from exponential to polynomial. *Second*, our model considers both static and adaptive contact networks. In the non-adaptive context, we derive key properties of the model. Under homogeneous mixing of the population, whereby all individuals are assumed to have direct contacts with each other, we obtain the expression for the basic reproduction number of our SI^aI^sS model. In the heterogeneous mixing case, where the contact network is arbitrary and directly modulates the spreading process, we establish that the individual infection probabilities in our SI^aI^sS model dominate those in the *SIS* model under similar conditions and derive an upper bound for the SI^aI^sS epidemic threshold. From these, we further derive the infection probability of each individual at the meta-stable state as a function of the effective recovery rate. *Finally*, for adaptive contact networks, the dynamics of the system are more complex and harder to analyze theoretically. To gain insights, we numerically explore the exclusive and combined effects of link adaptations, network topology, and asymptomatic infections on the epidemic prevalence and link density letting the model parameters span wide value ranges.

Formulating the SI^aI^sS Model

We focus on the simplest non-trivial model that tracks whether a node is infected or not (rather than all different states it might go through (*e.g.*, exposed, quarantined, isolated, hospitalized, dead)[25,26] while letting us model the co-evolution of the disease spreading and the network topology as the population adapts its behavior. Table 1 summarizes the key Mathematical notations used in this paper. We detail both aspects of the model next.

The SI^aI^sS model for static contact networks

In this section, we present the SI^aI^sS model. We abstract the population using a graph whose nodes represent individuals and links denote contacts between them. Specifically, we consider an underlying undirected network, $\mathscr{G}(\mathscr{V},\mathscr{E})$ with $\mathscr{V} = v_1,...,v_N$ the set of nodes (individuals) and $\mathscr{E} = e_1,...,e_L$ the set of links (contacts) where $N = |\mathscr{V}|$ and $L = |\mathscr{E}|$. $\mathscr{G}$ is represented by A, the $N \times N$ symmetric adjacency matrix, with $a_{n,m} = 1$ if there exists a link between nodes n and m and $a_{n,m} = 0$ otherwise. We also assume that G is connected, *i.e.*, there is a path between any pair of nodes in the network, so that A is irreducible.

We consider a disease that, at any point in time, partitions the population into three distinct groups:

- *Susceptible* individuals who are disease-free but prone to infection. Susceptible individuals have a chance of getting infected when contacting infected individuals, regardless of whether those are symptomatic or asymptomatic.
- *Asymptomatic Infected* individuals who are infected (and infectious) but do not exhibit any symptoms. These individuals appear to be healthy and do not trigger response from their contacts.
- *Symptomatic Infected* individuals who have been infected, are infectious and exhibit symptoms. These individuals may trigger reaction from their contacts.

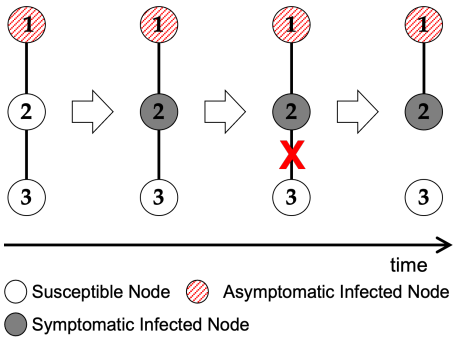

(a) Illustration of contact adaptation.

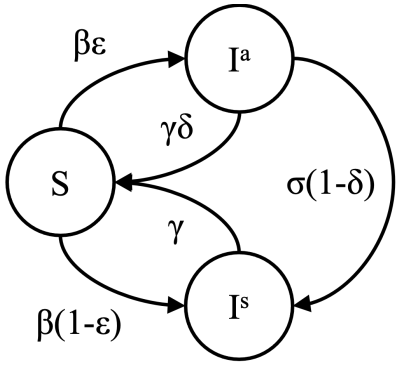

(b) State transition diagram for the SI^aI^sS model.

Figure 1. The SI^aI^sS model. (a) Illustration of contact adaptation: Node 1 is asymptomatic infectious. Node 2 continues to interact with node 1 due to unawareness and gets infected with symptoms. Node 3 avoids contact with node 2 once it detects the symptoms and thus avoids infection and remains susceptible. (b) the state transition diagram of the model.

Since each node must be in one of the three states at any given point in time, it holds that

$$s_n(t) + i_n^a(t) + i_n^s(t) = 1 \tag{1}$$

and

$$\frac{ds_n(t)}{dt} + \frac{di_n^a(t)}{dt} + \frac{di_n^s(t)}{dt} = 0 \tag{2}$$

Figure 1(a) illustrates how an asymptomatic individual (node 1) may cause a new infection (node 2) as well as how contact adaptation (*i.e.*, the break of the link between nodes 2 and 3) can prohibit further spread of the infection from node 2. Figure 1(b) then captures the state transition diagram of the proposed model. Both asymptomatic and symptomatic infected individuals infect a susceptible individual that contacts them at rate β. We use parameter ε to control the proportion of infections that are asymptomatic. In fact, some asymptomatic cases eventually exhibit infection symptoms; we control their proportion with parameter δ. In our model, an infected individual may exhibit symptoms with rate σ prior to recovering (that occurs at rate γ). Similarly, symptomatic individuals recover at rate γ. Following the literature, we assume that this transition from the infected to susceptible state is a Poisson process (*e.g.*, 27, 28). Furthermore, without loss of generality and unless otherwise specified, we use $\gamma = 1.0$ for the rest of the paper.

The network state at any time t can be defined by the combination of the states each of the N nodes resides in. As a result, the infection process can be identified as a continuous-time Markov Chain (CTMC) with 3^N states and be fully specified by a $3^N \times 3^N$ infinitesimal generator, $Q(t)$. The complexity of this CTMC becomes prohibitive even for small values of N, hence, we follow an important amount of literature in considering the individual node separately. When applying Markov theory at the node level, we obtain N instances of the infinitesimal generator, $Q_n(t)$, for the three-state CTMCs describing the transitions of each node:

$$Q_n(t) = \begin{bmatrix} -(q_{1,2;n} + q_{1,3;n}) & q_{1,2;n} & q_{1,3;n} \\ q_{2,1;n} & -(q_{2,1;n} + q_{2,3;n}) & q_{2,3;n} \\ q_{3,1;n} & 0 & -q_{3,1;n} \end{bmatrix}. \tag{3}$$

The recovery of infected node (*i.e.*, $q_{2,1;n}$ and $q_{3,1;n}$) and the emergence of symptoms upon infection (*i.e.*, $q_{2,3;n}$) are modeled as Poisson processes. The state transitions from susceptibility to asymptomatic infection (probabilities $q_{1,2;n}$), and symptomatic infection (probabilities $q_{1,3;n}$) are dependent on the states of other nodes in the network. To account for this dependency, both $q_{1,2;n}$ and $q_{1,3;n}$ must be conditioned on all possible combinations of states of all other network nodes. Unfortunately, this points back to the exact Markov chain solution of exponential complexity, as discussed earlier.

Following 28 and 29, we solve this problem by applying a mean-field approximation to the random variables, $q_{1,2;n}$ and $q_{1,3;n}$. Working with their expected rates, we reduce the complexity of the solution from exponential to polynomial.

With the mean-field approximation for $q_{1,2;n}$ and $q_{1,3;n}$, the effective infinitesimal generator can be written as:

$$\overline{Q_n(t)} = \begin{bmatrix} -(E[q_{1,2;n}] + E[q_{1,3;n}]) & E[q_{1,2;n}] & E[q_{1,3;n}] \\ \gamma\delta & -(\gamma\delta + \sigma(1-\delta)) & \sigma(1-\delta) \\ \gamma & 0 & -\gamma \end{bmatrix}. \tag{4}$$

In (4), $E[q_{1,2;n}]$ and $E[q_{1,3;n}]$ are the expected or effective infection rates of node, v_n, in the presence or absence of symptoms, respectively. They are functions of the infection rate, β and the states of v_n's neighbors. The information about the nodes' neighborhoods is encoded in the adjacency matrix, A. Node v_n is not immediately susceptible to infection until at least one of its neighbors is infected (with or without symptoms). The effective infection rates can then be written as:

$$E[q_{1,2;n}] = \beta\varepsilon \sum_{m=1}^{N} \left[a_{n,m}(t) \left(i_m^a(t) + i_m^s(t) \right) \right] \tag{5}$$

and

$$E[q_{1,3;n}] = \beta(1-\varepsilon) \sum_{m=1}^{N} \left[a_{n,m}(t) \left(i_m^a(t) + i_m^s(t) \right) \right]. \tag{6}$$

Applying the Markov differential equation (see 30, page 208), we obtain the following system of non-linear differential equations for $n \in \{1,...,N\}$

$$\frac{ds_n(t)}{dt} = -\beta \sum_{m=1}^{N} \left[a_{n,m}(t) \left(i_m^a(t) + i_m^s(t) \right) \right] s_n(t) + \delta\gamma i_n^a(t) + \gamma i_n^s(t), \tag{7}$$

$$\frac{di_n^a(t)}{dt} = \beta\varepsilon \sum_{m=1}^{N} \left[a_{n,m}(t) \left(i_m^a(t) + i_m^s(t) \right) \right] s_n(t) - \delta\gamma i_n^a(t) - \sigma(1-\delta) i_n^a(t), \tag{8}$$

$$\frac{di_n^s(t)}{dt} = \beta(1-\varepsilon) \sum_{m=1}^{N} \left[a_{n,m}(t) \left(i_m^a(t) + i_m^s(t) \right) \right] s_n(t) + \sigma(1-\delta) i_n^a(t) - \gamma i_n^s(t). \tag{9}$$

The spreading process is governed by this set of $3 \times N$ differential, which can be reduced to $2 \times N$, using Eq. 1. Solving them yields the instantaneous partition of the population into the three states.

Adaptive Contact Networks: Link Adaptation and the Network Evolution Process

In adaptive contact networks, the adjacency matrix, A, changes over time. We represent the temporally evolving network with $A(t)$, whose element $a_{n,m}(t)$ equals 1 if a link between nodes v_n and v_m exists at time t, and it equals 0, otherwise. We assume that no *new* contacts are established in the course of the epidemics (*i.e.*, $a_{n,m}(t) = 0, \forall t$, if $a_{n,m}(0) = 0$). The network topology evolves based on two independent processes as follows:

- *Link-breaking process* – a node without symptoms, *i.e.*, a node in either the susceptible or asymptomatic infected state, avoids contacts with a node exhibiting infection symptoms. Specifically, a non-symptomatic node v_n will break the existing link with a neighboring node v_m with Poisson rate ζ if v_m gets infected and develops symptoms.
- *Link-creation process* – conversely, if both end nodes of a link that broke earlier, because at least one of the two nodes got infected and developed symptoms, do not (any more) exhibit symptoms, the link between them is re-established with Poisson rate ξ.

We follow the methodology described in 20 to model the link adaptation processes. Specifically, we define two functions, f_{br} and f_{cr}, describing the link-breaking and link-creation mechanisms, respectively. The two link adaptation processes are solely dependent on the states of the two link end-point nodes. Since in our SI^aI^sS model each node can be in one of three states at any point in time, there are six distinct combinations of states for each pair of nodes. Table 2 lists those six combinations and the associated actions. From the table, we note that susceptible and asymptomatic infected nodes induce the same actions and thus can be grouped together. Then, the link adaptation action is simply determined by whether the end nodes of a link are symptomatic infected. Let $X_n(t)$ be the Bernoulli random variable indicating whether node n is symptomatic infected at time t ($X_n(t) = 1$) or not ($X_n(t) = 0$). Following 20, we obtain the following expressions:

$$f_{br}(X_n(t), X_m(t)) = X_n(t) + X_m(t) - 2X_n(t)X_m(t), \tag{10}$$

$$f_{cr}(X_n(t), X_m(t)) = 1 - X_n(t) - X_m(t) + X_n(t)X_m(t). \tag{11}$$

Hence, a link between two nodes m, n breaks (with rate ζ) when either one of the two is symptomatic infected and is created (with rate ξ) when both of them lie in a state other than the Symptomatic Infected one.

Table 2. Link break/creation rules by time t for two nodes v_n, v_m with $a_{n,m}(0) = 1$, depending on current $a_{n,m}(t)$

State v_n	State v_m	$a_{n,m}(t)$	Action
S	S	0	Create link
		1	No action
S	I^a	0	Create link
		1	No action
S	I^s	1	Break link
		0	No action
I^a	I^a	0	Create link
		1	No action
I^a	I^s	1	Break link
		0	No action
I^s	I^s	0, 1	No action

We apply a mean-field approximation by taking the expectation on both sides, with $E[X_n(t)] = Pr[X_n(t) = 1] = i_n^s(t)$. Following 31, we assume that the random variables $X_n(t)$ and $X_m(t)$ are uncorrelated (*i.e.*, $E[X_n(t)X_m(t)] = E[X_n(t)]E[X_m(t)]$) for all $n \neq m$. As a result, the equations that govern the evolution of link $a_{n,m}$ are obtained as Eq. 12,

$$\frac{da_{n,m}(t)}{dt} = a_{n,m}(0)\Big[-\zeta a_{n,m}(t) f_{br}(i_n^s(t), i_m^s(t)) + \xi\big(1 - a_{n,m}(t)\big) f_{cr}(i_n^s(t), i_m^s(t))\Big], \tag{12}$$

where $s_n(t)$, $i_n^a(t)$ and $i_n^s(t)$ denote the probabilities that node n resides in the susceptible (S), asymptomatic infected (I^a) and symptomatic infected (I^s) states at time t, respectively. Note that the interaction between the two end nodes of a link is assumed to be symmetric, thus preserving the symmetry of the adjacency matrix $A(t)$.

Epidemic Threshold and Prevalence

One important quantity of interest when studying epidemic spreading is its prevalence (*i.e.*, the fraction of infected population). We can compute the prevalence of the epidemic at time t in the network as follows:

$$\rho(t) = \frac{1}{N}\sum_{n=1}^{N}\Big(i_n^a(t) + i_n^s(t)\Big). \tag{13}$$

With our individualized modelling approach, we can also compute individual infection probabilities (*i.e.*, $i_n^a(t) + i_n^s(t)$ and $i_{n\infty}^a + i_{n\infty}^s$). Thus, we do not only obtain the prevalence as an aggregate value for the entire network, but also gain insights into the susceptibility of individual nodes.

We are also interested in understanding the epidemic threshold, *i.e.*, the point above which the epidemic will almost surely spread. For this purpose, in the following, we derive the basic reproduction number $\mathscr{R}_0$ of our SI^aI^sS model, which indicates the expected number of secondary infections produced by a single infected individual in a completely susceptible population[32]. When $\mathscr{R}_0 < 1.0$, one infected node infects less than one node on average and the epidemic dies out. Conversely, when $\mathscr{R}_0 > 1.0$, an infected node is capable of infecting more than one susceptible node on average and the epidemic escalates.

Numerical Results and Discussion

We first provide some insights into the SI^aI^sS model in a non-adaptive setup, where the nodes do not adapt their connections with their neighbors (*i.e.*, $\zeta = \xi = 0$). By switching off the link adaptation mechanism, both symptomatic and asymptomatic nodes infect their neighbors in a similar manner since healthy neighbors are immediately susceptible to infection without the ability to avoid contacts. In this analysis, we draw parallels with the classical SIS model, to which our SI^aI^sS model can be reduced to by setting $\delta = 1.0$.

We first investigate the case of homogeneous mixing, as this results from the law of mass action. The contact graph is complete, *i.e.*, $a_{n,m} = 1, \forall n, m \in \mathscr{V}, n \neq m$ and $a_{n,n} = 0, \forall n \in \mathscr{V}$ so that each node is in direct and constant contact with all other nodes and the network topology does not affect the spreading process. We adopt the next generation matrix approach[33] to compute $\mathscr{R}_0$ under homogeneous mixing. In the absence of adjacency matrix elements and for $\xi = \zeta = 0$, the system of differential equations (7)-(9) and (12) is simplified as follows:

$$\frac{dS}{dt} = -\beta(I^a + I^s)S + \delta\gamma I^a + \gamma I^s, \tag{14}$$

$$\frac{dI^a}{dt} = \beta\varepsilon(I^a + I^s)S - \delta\gamma I^a - \sigma(1-\delta)I^a, \tag{15}$$

$$\frac{dI^s}{dt} = \beta(1-\varepsilon)(I^a + I^s)S + \sigma(1-\delta)I^a - \gamma I^s, \tag{16}$$

$$\frac{dA}{dt} = 0. \tag{17}$$

In the SI^aI^sS model, the transitions $S \to I^a$ and $S \to I^s$ mark new infections and both states I^a and I^s are *states-at-infection*, *i.e.*, states that individuals occupy immediately upon their infection[33]. On the contrary, the transition $I^a \to I^s$ does not generate new infections but rather marks the progression of already infected nodes to a different infection state. The computation of the next generation matrix $\mathscr{K}$ and, eventually, $\mathscr{R}_0$ involve only the two states-at-infection. Linearizing equations (15) and (16) around the infection-free steady-state $(S = N, I^a = I^s = 0)$, we can derive the linearized infection subsystem in matrix form

$$\begin{bmatrix} \frac{dI^a}{dt} \\ \\ \frac{dI^s}{dt} \end{bmatrix} = \begin{bmatrix} \beta\varepsilon - \delta\gamma - \sigma(1-\delta) & \beta\varepsilon \\ \\ \sigma(1-\delta) + \beta(1-\varepsilon) & \beta(1-\varepsilon) - \gamma \end{bmatrix} \begin{bmatrix} I^a \\ \\ I^s \end{bmatrix}, \tag{18}$$

where the 2×2 matrix on the right hand side of (18) is the Jacobian matrix of the original system of nonlinear equations (15) and (16). We can then write the Jacobian matrix as the sum of matrix F corresponding to transmission events (generation of new infections) and the matrix V corresponding to transitions between infected states and recovery to state S, where:

$$F = \begin{pmatrix} \beta\varepsilon & \beta\varepsilon \\ \beta(1-\varepsilon) & \beta(1-\varepsilon) \end{pmatrix} \qquad \text{and} \qquad V = \begin{pmatrix} \delta\gamma + \sigma(1-\delta) & 0 \\ -\sigma(1-\delta) & \gamma \end{pmatrix},$$

where F is non-negative and V is a non-singular matrix. We can then compute the next generation matrix, $\mathscr{K}$, in line with 33

$$\mathscr{K} = FV^{-1} = \begin{pmatrix} \frac{\beta\varepsilon(\gamma+\sigma(1-\delta))}{\gamma(\gamma\delta+\sigma(1-\delta))} & \frac{\beta\varepsilon}{\gamma} \\ \\ \frac{\beta(1-\varepsilon)(\gamma+\sigma(1-\delta))}{\gamma(\gamma\delta+\sigma(1-\delta))} & \frac{\beta(1-\varepsilon)}{\gamma} \end{pmatrix}, \tag{19}$$

where V^{-1} denotes the inverse of matrix V. Then, $\mathscr{R}_0$ equals the largest eigenvalue of $\mathscr{K}$, which can be computed out of the trace and the determinant of $\mathscr{K}$:

$$\mathscr{R}_0 = \lambda_1(\mathscr{K}) = \frac{1}{2}(tr(\mathscr{K}) + \sqrt{tr^2(\mathscr{K}) - 4\,det(\mathscr{K})}\,)$$

and since $det(\mathscr{K}) = 0$, we get

$$\mathscr{R}_0 = \frac{\beta}{\gamma}\left(\frac{\sigma(1-\delta) + \delta\gamma + \varepsilon\gamma - \delta\varepsilon\gamma}{\delta\gamma + \sigma(1-\delta)}\right) = \frac{\beta}{\gamma}\left(1 + \frac{\varepsilon\gamma(1-\delta)}{\delta\gamma + \sigma(1-\delta)}\right) \geq \frac{\beta}{\gamma} \quad \forall\gamma, \delta, \varepsilon. \tag{20}$$

Note we can revert back to the original *SIS* model by setting $\delta = 1$, *i.e.*, eliminating the discrimination between the I^a and I^s states. For $\delta = 1$, $\mathscr{R}_0$ reduces to the basic reproduction number β/γ of the *SIS* model. Moreover, simple algebraic calculations yield that $\frac{\partial\mathscr{R}_0}{\partial\delta} < 0$, *i.e.*, other things held constant, the higher the percentage of asymptomatic nodes that recover before developing symptoms, the smaller the reproduction number.

Heterogeneous Mixing in Non-adaptive networks

We, then, relax the homogeneous mixing assumption so that the underlying network graph is no longer complete. The nodes' contacts are still fixed ($\zeta = \xi = 0.0$) but they can now be encoded in an arbitrary adjacency matrix A.

Similar to the classical N-intertwined *SIS* model[28], the SI^aI^sS model possesses the trivial solution $i_{n\infty} = i^a_{n\infty} + i^s_{n\infty} = 0$ (no infected nodes in the network) in the asymptotic regime $t \to \infty$ since the Markov chain is finite and possesses an absorbing state that is reachable by all other states. In practice, for any network of realistic size, it has been found that the asymptotic solution *may* only be reached after a very long period during which the system converges exponentially fast to another stable state, often referred to as the "meta-stable state", and remains there for most of the time[28,34]. The condition that determines whether the spreading process will indeed converge to this meta-stable state is related to the spectral radius of the adjacency matrix representing the network. Specifically for the N-intertwined *SIS* model, the spreading process evolves to epidemic and converges to the meta-stable state if

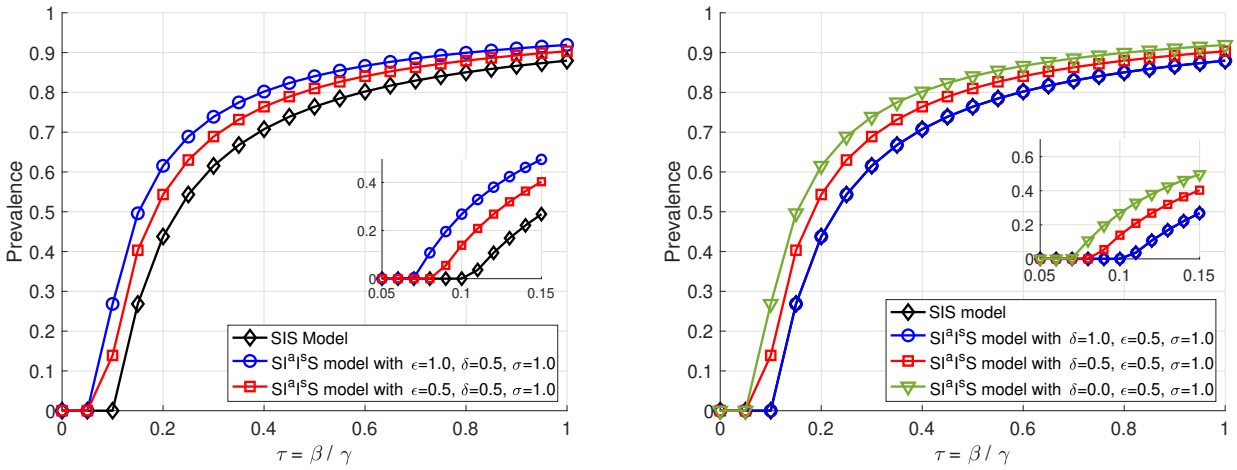

(a) $\delta = 0.5$, $\sigma = 1$, variable ε. **(b)** $\varepsilon = 0.5$, $\sigma = 1$, variable δ.

Figure 2. *SIS* vs SI^aI^sS model in non-adaptive setting ($\zeta = \xi = 0$).

$$\tau = \beta/\gamma > 1/\lambda_1(A), \tag{21}$$

where $\lambda_1(A)$ is the largest eigenvalue of A and $1/\lambda_1(A) \doteq \tau_c^{SIS}$ the epidemic threshold of the model[28,35,36]. At the meta-stable state, the individual infection steady-state probabilities p_n^{ss} satisfy the system of equations

$$\frac{\beta}{\gamma}\sum_{m=1}^{N} a_{n,m}p_m^{ss} = \frac{p_n^{ss}}{1-p_n^{ss}}. \tag{22}$$

We can make two remarks regarding the way the SI^aI^sS model compares to the N-intertwined *SIS* model, codified below as propositions for easier reference. Let

$$i_n(t) = i_n^a(t) + i_n^s(t) \tag{23}$$

be the overall infection probabilities of individuals, where the infected population is the sum of symptomatic and asymptomatic individuals. We can show that:

Proposition 1. *For two spreading processes, $p_n(t), i_n(t)$, evolving under the SIS and SI^aI^sS models, respectively, sharing the same underlying graph and starting from the same initial conditions, i.e., $i_n(t_0) = p_n(t_0), n \in \mathcal{V}$, the infection probabilities of individuals in the two models satisfy $p_n(t) \leq i_n(t), n \in \mathcal{V}$ $\forall t \in [t_0, \infty]$.*

Refer to Supplementary Appendix A for the corresponding proof.

Following this, we can also state that:

Corollary 1. *The SIS epidemic threshold serves as an upper bound for the SI^aI^sS epidemic threshold, i.e.,*

$$\tau_c^{SI^aI^sS} \leq \tau_c^{SIS} = 1/\lambda_1(A). \tag{24}$$

Refer to Supplementary Appendix A for the corresponding proof.

In Fig. 2(a), we compare the epidemic prevalence of the SI^aI^sS to the *SIS* model, for $\varepsilon = \{1.0, 0.5\}$ and $\sigma = \delta = 0.5$. We see that higher proportion of asymptomatic nodes (*i.e.*, higher ε) leads to higher epidemic prevalence. We also see that the epidemic begins to spread at lower values of the $\tau = \beta/\gamma$ ratio (see inset of Fig. 2(a)), in line with (20). This is a result of the increased overall time a node spends in infection states thanks to the additional state transition from I^a to I^s. This also corroborates our statement above regarding the domination of SI^aI^sS over *SIS* model.

Proposition 2. *The steady-state probabilities of individuals at the meta-stable state of the SI^aI^sS model satisfy the equations:*

$$\frac{\beta}{\gamma_{eff}}\sum_{m=1}^{N} a_{n,m}i_m^{ss} = \frac{i_n^{ss}}{1-i_n^{ss}}, \tag{25}$$

where

$$\gamma_{eff} = \frac{\gamma}{1+\frac{\varepsilon\gamma(1-\delta)}{\delta\gamma+\sigma(1-\delta)}} < \gamma. \tag{26}$$

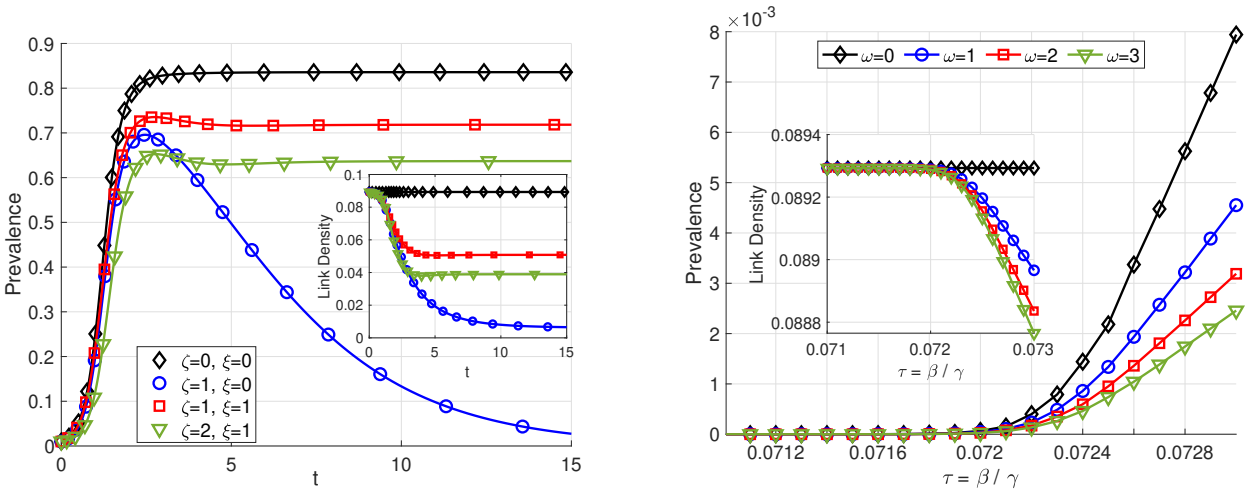

(a) Prevalence and link density (inset) of the SI^aI^sS model. **(b)** Focused around threshold region for $\omega = \{0,1,2,3\}$.

Figure 3. Impact of different link adaptation scenarios based on the SI^aI^sS model.

Refer to Supplementary Appendix A for the corresponding proof.

Comparing (25) with its *SIS* counterpart in (22), the SI^aI^sS model could be viewed as an *SIS* model, *i.e.*, with a single infection state, the same infection rate β and recovery rate γ_{eff}, smaller than the original *SIS* recovery rate γ.

Figure 2(b) compares the epidemic prevalence under the *SIS* and SI^aI^sS models as δ varies from 0 to 1. For $\delta = 1$, the prevalence curves for the two models overlap since the SI^aI^sS model reduces to the *SIS* one. As δ varies from 1 down to 0, the spreading process takes off at lower τ values (see inset) and the prevalence scores distinctly higher than under the *SIS* model.

Heterogeneous Mixing in Adaptive Networks

We numerically explore the implications of different link adaptations, network topology features and the asymptomatic infected population on the epidemic dynamics. As our baseline scenario, we set $\beta = 0.5$, $\gamma = 1.0$, $\varepsilon = 0.5$ (i.e., we assume that 50% of new infections are asymptomatic), $\delta = 0.5$ (i.e., 50% of those asymptomatic cases developing symptoms), $\sigma = 0.1$, $\xi = \zeta = 1.0$. We vary the effective spreading rate by fixing γ and changing β. Unless otherwise stated, we experiment with random graphs of $N = 100$ nodes and link probability $p = 2 \times ln(N)/N$, which drives the probability that the graph is connected to 1 as N tends to infinity.

Impact of Link Adaptations

From our analysis for the case of heterogeneous mixing in non-adaptive networks, we established that, in non-adaptive setting, $1/\lambda_1(A)$ sets an upper bound on the epidemic threshold for our SI^aI^sS model. However, as soon as we consider link adaptiveness, *i.e.*, nodes avoiding contacts with symptomatic infected nodes, the adjacency matrix changes over time, and consequently, its eigenvalues and corresponding eigenvectors are also time-dependent functions. Since there are no new link establishments, we have $a_{n,m}(0) \geq a_{n,m}(t)\ \forall n,m,t$. As $A(t)$ is always a non-negative square matrix, it follows from the Perron-Frobenius theorem that $\lambda_1(A(0)) \geq \lambda_1(A(t))\ \forall t > 0$. From this, we can also conjecture that the upper bound of the SI^aI^sS epidemic threshold is higher in the adaptive setting than it is in the non-adaptive setting.

In Fig. 3(a), we plot the epidemic prevalence and link density (inset) under four different link adaptation settings in the baseline scenario: (1) nodes do not adapt at all their contacts ($\diamondsuit$), (2) nodes break links with infected contacts but do not reconnect after recovering ($\bigcirc$) (3) link breaking and creation rates are equal ($\square$) and (4) the link breaking rate is twice the link creation rate ($\bigtriangledown$). Clearly, a population without contact adaptation (*i.e.*, $\zeta = 0$) allows wider spread of the epidemic. Population that actively avoids contacts with symptomatic nodes inhibits the epidemic spreading and results in lower prevalence. However, this also isolates the population as it can be seen in the decrease of the link density.

To explore the epidemic threshold region, we define the *effective link-breaking rate* $\omega = \frac{\zeta}{\xi}$ ($\omega = 0.0$ implies that link adaptation is disabled). In Fig. 3(b) we show the co-evolution of the epidemic prevalence and link density around the threshold region. Interestingly, our SI^aI^sS model portrays a fixed epidemic threshold, or bifurcation parameter, which is independent of the effective link-breaking rate, ω. A similar observation is made in 31 for the adaptive *SIS* (*ASIS*) model, first introduced in 37 with complete original contact graph $A(0)$: the transcritical bifurcation parameter they compute via the first-order mean-field approximation is fixed for different effective link-breaking rates, ω. However, 31 further reports that the epidemic threshold appears to scale linearly with ω when the second-order mean-field approximation is considered, so that our experimental

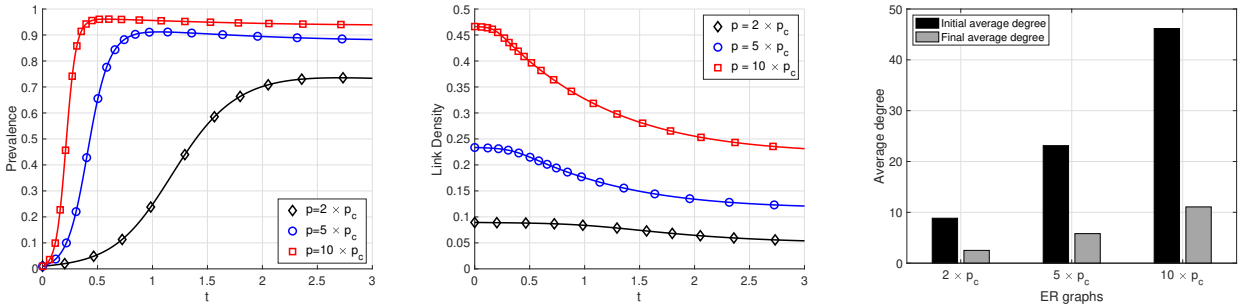

(a) Prevalence for ER networks with different link density.

(b) Link density evolution over time for the three networks.

(c) Average degree before and after epidemic spreading.

Figure 4. Impact of link density.

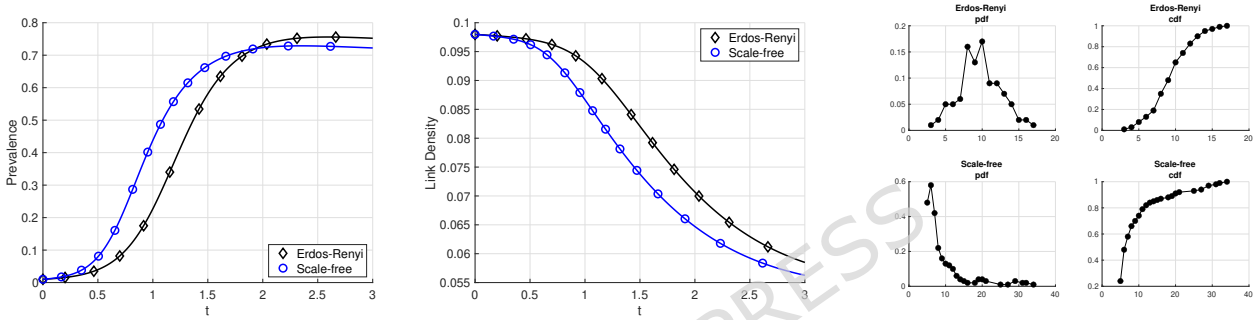

(a) Prevalence evolution over time.

(b) Link density evolution over time.

(c) Node degree pdf (left) and cdf (right).

Figure 5. Impact of degree distribution on prevalence and link density; experiments with ER and Scale-Free networks.

evidence here about the threshold invariance is definitely not conclusive. In general, we find that higher effective link-breaking rate, ω, results in lower link density (*i.e.*, more susceptible nodes break links with observable infected nodes) and prevalence (*i.e.*, more link breaking inhibits the epidemic spreading).

Impact of Network Topology

In this section, we show how network topology affects the actual spreading dynamics. We first examine the influence of the initial density of the contact network. We generate ER graphs with three different link densities (*i.e.*, $2 \times p_c$, $5 \times p_c$ and $10 \times p_c$). Figure 4(a) clearly suggests that higher link densities facilitate faster spreading and higher epidemic prevalence. The lower the parameter p value the slower the epidemic prevalence growth and the lower its value reached at steady-state. Likewise, for higher link probability p, the link density drops more drastically from its initial value towards its steady-state value, as shown in Fig. 4(b). This more dramatic change in the network topology as the original link density increases is also reflected in the comparison of the average node degrees between $t = 0$ and after the epidemic prevalence value stabilizes. As shown in Fig. 4(c), higher density networks experience higher decrease in average degree.

Nevertheless, networks with identical link density at $t = 0$, may also experience different epidemic dynamics. To illustrate this, we use two networks with the same number of links but different degree distributions. The first network follows the ER model[38] with the binomial degree distribution whereas the second network follows the scale-free model[39] featuring power-law degree distributions. (cf. Fig. 5(c) where the top row depicts the probability and cumulative density functions (pdf and cdf) of node degrees for a sample ER network and the bottom row depicts the same for a sample scale-free network). The hub nodes in the scale-free network, *i.e.*, those nodes featuring many more direct neighbors than others and giving rise to the right heavy tail in the degree distribution, help the epidemic spread faster (see Fig. 5(a)). However, interestingly, the stable prevalence level is lower than that of the ER graph, and, as Fig. 5(b) suggests, so is the link density over time. As hub nodes enter the symptomatic infected state and their neighbors start avoiding contacts with them, the link breaking events are more frequent.

Impact of Asymptomatic Infections

The next set of results focus on the effect of asymptomatic nodes in an adaptive network. We return to our baseline scenario and control the asymptomatic infected population via parameter ε. We consider four cases: (a) $\varepsilon = 0$: with symptomatic infected

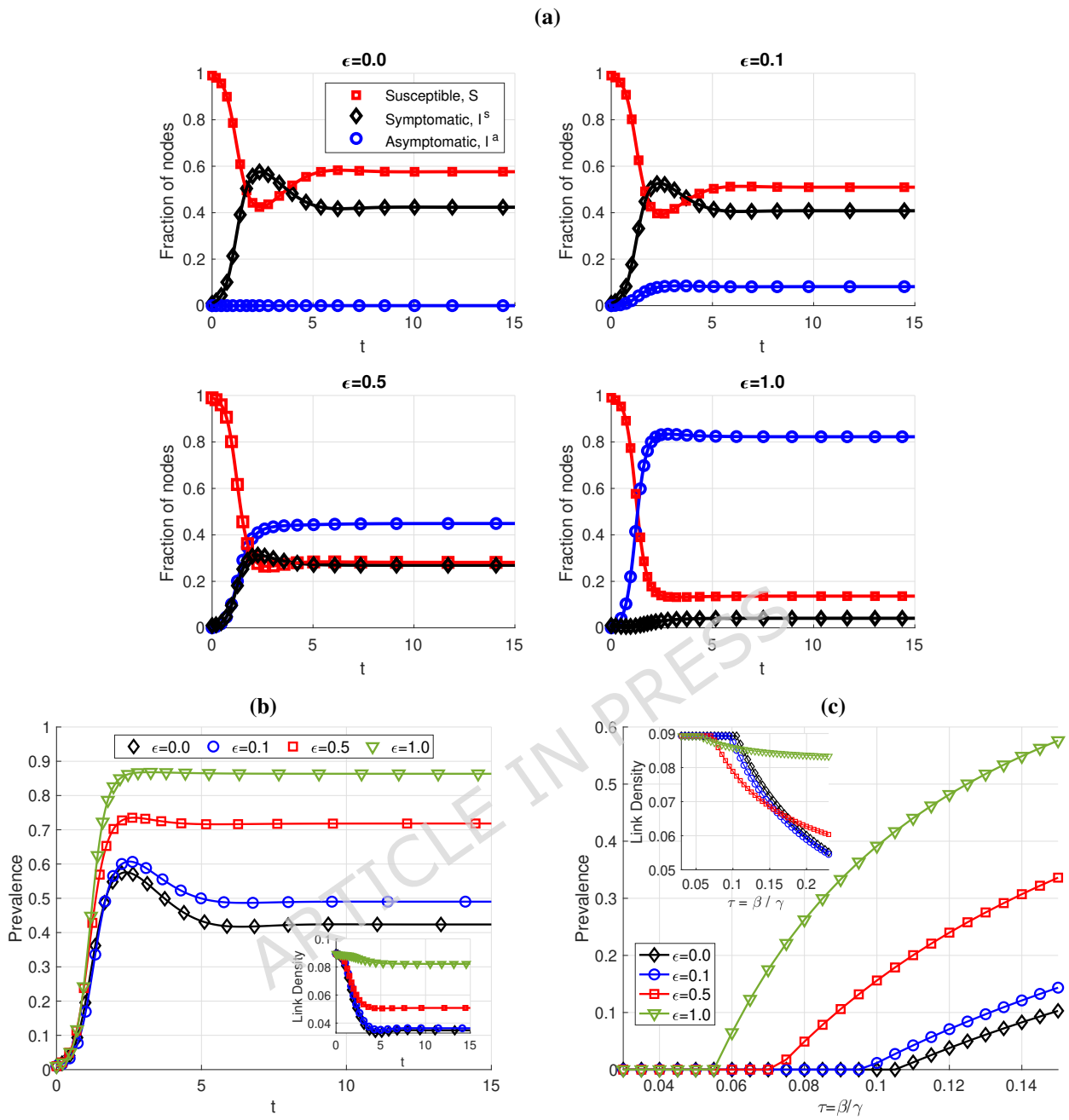

Figure 6. (a) Time evolution of SI^aI^sS for the baseline scenario with asymptomatic infection rates, $\epsilon = \{0.0, 0.1, 0.5, 1.0\}$; (b) Prevalence for the corresponding ϵ values; (c) Prevalence and link density around the threshold region for the same ϵ values.

seed node, resulting in no asymptomatic nodes and reduces to the *SIS* model, (b) $\epsilon = 0.1$: low generation rate of asymptomatic nodes upon infection, (c) $\epsilon = 0.5$: equal probabilities to develop or not symptoms upon infection, and (d) $\epsilon = 1.0$: all infections start without symptoms. Figure 6(a) plots the characteristic curves of SI^aI^sS for the four cases and Fig. 6(b) compares the corresponding prevalence and link density (inset) trajectories over time. We see that higher numbers of asymptomatic infections restrict harder the nodes' capacity to adapt to the ongoing epidemic (*i.e.*, breaking links with infected nodes), resulting in higher link density even at the same effective link breaking rate, $\omega = 1$, for all cases. Consequently, the epidemic prevalence grows hand-in-hand with the number of asymptomatic infected nodes, which catalyze the epidemic process in two ways: by lengthening the duration of infection (when $\delta < 1$) and by reducing the effective link breaking rate.

In contrast to the the first order approximation results discussed in the Section on the Impact of Link Adaptations, which indicate that the epidemic threshold is insensitive to the effective link-breaking rate ω (cf. Fig. 3(b)), the epidemic threshold

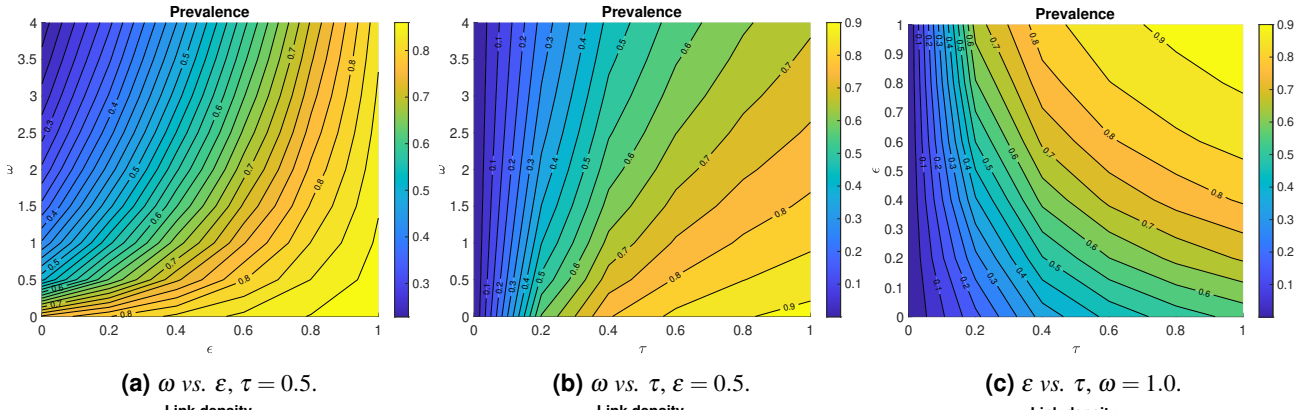

(a) ω *vs.* ε, $\tau = 0.5$. **(b)** ω *vs.* τ, $\varepsilon = 0.5$. **(c)** ε *vs.* τ, $\omega = 1.0$.

(d) ω *vs.* ε, $\tau = 0.5$. **(e)** ω *vs.* τ, $\varepsilon = 0.5$. **(f)** ε *vs.* τ, $\omega = 1.0$.

Figure 7. Contour maps of epidemic prevalence (top row) and corresponding link density (bottom row) for three settings: (first column) ω *vs.* ε, (second column) ω *vs.* τ and (third column) ε *vs.* τ.

appears to scale inversely with ε. We show this in Fig. 6(c) zooming in on the τ threshold region, where the epidemic threshold decreases for higher ε values. Fig. 6(c)(inset) shows the link density for the four cases.

Modulated Effects

We know that higher $\tau = \beta/\gamma$ values result in higher epidemic prevalence. From above, we also understand that the epidemic prevalence drops as the effective link-breaking rate, ω, increases or asymptomatic infections get sparser (*i.e.*, low ε). Here, we investigate the modulated effect of these three parameters (τ, ω, ε) producing three sets of contour maps, as shown in Fig. 7. In the first set of results, Fig. 7(a) and (d), we show the contour maps of prevalence and link density, respectively, under a range of (ω, ε) combinations (the remaining parameters follow the baseline scenario). As we increase the two parameters, the prevalence and link density follow different paths: high effective link-breaking rate inhibits spreading (top-left corner of Fig. 7(a)), whereas high percentage of asymptomatic nodes favors it (bottom-right corner). Both the prevalence and link density increase diagonally from top-left towards the bottom-right corner in the contour maps under the opposite effect of ω and ε.

Fig. 7(b) and (e) plot the prevalence and link density contour maps for (ω, τ) value pairs. The two parameters have opposite impact on the prevalence but similar impact on the link density (*i.e.*, prevalence (link density) increases (resp. decreases) as τ increases and ω decreases (resp. increases)). Comparing the link densities in Fig. 7(d) and (e), the contour map is 'flipped' along the vertical axis. The highest link density is achieved at opposite bottom corners. As opposed to the ω *vs.* ε case, where prevalence and link density are strongly positively correlated as we vary ω and ε, in the ω *vs.* τ case, increasing either ω or τ strengthens the link breaking process. In this case, we witness (very) low prevalence scores coupled with high link density values (left side of contour maps) or high prevalence coupled with (very) low link density (top-right corner of contour maps).

In the last set of contour maps, in Fig. 7(c) and (f), we look into the ε *vs.* τ relation. Both parameters are positively correlated with prevalence, whereas they differ with respect to link density: τ is negatively correlated while ε is positively correlated with it. As a result, the highest prevalence is obtained at the top-right corner of the contour map in Fig. 7(c), whereas the lowest link density appears at the bottom-right corner of the contour map, when the τ is highest and ε is lowest. Analyzing across the three sets of results, we observe that τ is the dominant determinant for low prevalence with ε and ω having little effect at this region. However, ε emerges to be the main contributing factor at high epidemic prevalence. The neutralizing effect from tuning ω fails at high prevalence region with high number of asymptomatic silent spreaders.

Conclusions

We study the spreading process involving (a) nodes who may not exhibit symptoms themselves when they get infected; and, (b) may break contacts with other nodes in their social network when those exhibit infection symptoms. Our goal is to study the dynamics of the diffusion processes that emerge when undetectable infectious nodes hamper the network's ability to defend against the epidemic spread by breaking contacts. Our compartmental SI^aI^sS model breaks down the network population into three distinct compartments (*i.e.*, Susceptible, Asymptomatic infected and Symptomatic infected). We employ CTMC analysis to model the spreading process by taking into account the state transitions of individual nodes rather than the aggregate behavior of all nodes. We apply a mean-field approximation to reduce the complexity of the solution from exponential (exact solution) to polynomial.

We pursue our goal by working in three stages of progressively higher analysis complexity. In the first stage, we consider a homogeneous mixing network whereby all nodes have direct contacts with each other that do not change in the course of the spreading process. For this network, we draw on the next generation matrix approach to derive its basic reproduction number, $\mathscr{R}_0$ (*i.e.*, Eq. 20). Then, we consider a non-adaptive heterogeneous mixing setup with the contact network represented by an adjacency matrix. Here, we contrast our SI^aI^sS model against the classical N-intertwined SIS model[28]. We find that our model dominates the N-intertwined SIS model in terms of individual infection probabilities and obtain an upper bound for its epidemic threshold. We derive the effective recovery rate from the two infectious states in our model, which is shown to be smaller than the one of the SIS model and formulate a system of equations for the individual infection probabilities at the metastable state that is reminiscent of the one for the original SIS model.

Finally, we explore our model in the contact-adaptive setting, investigating how individual parameters and their combinations affect the trajectories of epidemic prevalence and link density of the network over time. We find that the retarding effect of the link-breaking mechanism upon the spreading process is far less effective in the presence of asymptomatic infected nodes who cannot be detected and avoided by healthy nodes. Our analysis and results further corroborate recent empirical observations that epidemics with an asymptomatic infectious period feature higher epidemic prevalence even when counter-measures such as isolation and quarantine are in effect. This serves as a strong indication of how even such a general model can offer insights not captured by classical epidemic models and could inform the formulation of policies and/or counter-measure design based specific application context. Such implications for policy design would apparently be more detailed and precise if the model is extended to account for other states such as exposed (analogous to $SEIR$ model[32]), quarantined, hospitalized, but in all cases, the additional detail would need to be traded with extra complexity and weaker approximations of exact solutions. On a more technical front, our work here has drawn heavily on first order mean-field approximations of the CTMC. While this has offered various insights into the spreading dynamics under different mix of asymptomatic population and link-breaking rates, we conjecture that better estimates of the epidemic threshold could be obtained with higher-order approximations. For instance, 31 and 19 reported good qualitative approximation for the basic SIS model in contact adaptive setting using second-order mean-field approximations.

References

1. Coronavirus: The mystery of asymptomatic 'silent spreaders'. https://www.bbc.co.uk/news/uk-52840763. Accessed: 13-02-2025.
2. Kolias, C., Kambourakis, G., Stavrou, A. & Voas, J. Ddos in the iot: Mirai and other botnets. IEEE Comput. Soc. **50**, 80–84 (2017).
3. Scaife, N., Traynor, P. & Butler, K. Making sense of the ransomware mess (and planning a sensible path forward). IEEE Potentials **36**, 28–31, DOI: 10.1109/MPOT.2017.2737201 (2017).
4. Acarali, D., Rajarajan, M., Komninos, N. & Zarpelao, B. B. Modelling the spread of botnet malware in iot-based wireless sensor networks. Secur. Commun. Networks **2019**, DOI: 10.1155/2019/3745619 (2019).
5. Robinson, M. & Stilianakis, N. I. A model for the emergence of drug resistance in the presence of asymptomatic infections. Math. Biosci. **243**, 163–177, DOI: https://doi.org/10.1016/j.mbs.2013.03.003 (2013).
6. Ansumali, S., Kaushal, S., Kumar, M. K., A. Prakash & Vidyasagar, M. Modelling a pandemic with asymptomatic patients, impact of lockdown and herd immunity, with applications to sars-cov-2. Annu. Rev. Control. **50**, 432–447 (2020).
7. Chen, Y.-C., Lu, P.-E., Chang, C.-S. & Liu, T.-H. A time-dependent sir model for covid-19 with undetectable infected persons. IEEE Trans. Netw. Sci. Eng. **7** (2020).
8. D'Andrea, V., Gallotti, R., Castaldo, N. & De Domenico, M. Individual risk perception and empirical social structures shape the dynamics of infectious disease outbreaks. PLoS Comput. Biol. **18(2):e1009760** (2022).
9. Gaeta, G. A simple SIR model with a large set of asymptomatic infectives. Math. Eng. **3**, 1–39 (2020).
10. Dobrovolny, H. M. Modeling the role of asymptomatics in infection spread with application to SARS-CoV-2. PLoS ONE **15(8):e0236976** (2020).
11. Espinoza, B., Marathe, M., Swarup, S. & Thakur, M. Asymptomatic individuals can increase the final epidemic size under adaptive human behavior. Nat. Sci. Reports **11:19744** (2021).
12. Taylor, M., Taylor, T. J. & Kiss, I. Z. Epidemic threshold and control in a dynamic network. Phys. Rev. E **85**, DOI: 10.1103/physreve.85.016103 (2012).
13. Kermack, W. O. & McKendrick, A. G. A contribution to the mathematical theory of epidemics. Proc. Royal Soc. A: Math. Phys. Eng. Sci. **115** (1927).

14. Holme, P. Temporal network structures controlling disease spreading. Phys. Rev. E **94**, DOI: 10.1103/PhysRevE.94.022305 (2016).

15. Cai, C.-R., Nie, Y.-Y. & Holme, P. Epidemic criticality in temporal networks. Phys. Rev. Res. **6**, L022017, DOI: 10.1103/PhysRevResearch.6.L022017 (2024).

16. Gross, T., Dommar, C. & Blasius, B. Epidemic dynamics on an adaptive network. Phys. Rev. Lett. **96**, 208701, DOI: 10.1103/PhysRevLett.96.208701 (2006).

17. Bodó, A. & Simon, P. Analytic study of bifurcations of the pairwise model for sis epidemic propagation on an adaptive network. Differ Equ Dyn Syst **28**, 807–826 (2020).

18. Liu, C., Zhou, N., Zhan, X., Sun, G. & Zhang, Z. Markov-based solution for information diffusion on adaptive social networks. Appl. Math. Comput. **380, 125286** (2020).

19. Kiss, I. Z., Berthouze, L., Taylor, T. J. & Simon, P. L. Modelling approaches for simple dynamic networks and applications to disease transmission models. Proc. Royal Soc. A **468**, 1332–1355 (2012).

20. Achterberg, M. A., Dubbeldam, J. L. A., Stam, C. J. & Van Mieghem, P. Classification of link-breaking and link-creation updating rules in susceptible-infected-susceptible epidemics on adaptive networks. Phys Rev E **101** (2020).

21. Braun, B., Taraktaş, B., Beckage, B. & Molofsky, J. Simulating phase transitions and control measures for network epidemics caused by infections with presymptomatic, asymptomatic, and symptomatic stages. PLOS ONE **15**, 1–14, DOI: 10.1371/journal.pone.0238412 (2020).

22. Hota, A. R. & Gupta, K. A generalized sis epidemic model on temporal networks with asymptomatic carriers and comments on decay ratio. In 2021 American Control Conference (ACC), 3176–3181, DOI: 10.23919/ACC50511.2021.9483218 (2021).

23. Moradian, M., Dadlani, A., Kairgeldin, R. & Khonsari, A. Cost-effective activity control of asymptomatic carriers in layered temporal social networks. IEEE Transactions on Comput. Soc. Syst. **12**, 1969–1982, DOI: 10.1109/TCSS.2024.3392715 (2025).

24. Pastor-Satorras, R., Castellano, C., Van Mieghem, P. & Vespignani, A. Epidemic processes in complex networks. Rev. Mod. Phys. **87** (2015).

25. Van den Driessche, P. & Watmough, J. Reproduction numbers and sub-threshold endemic equilibria for compartmental models of disease transmission. Math. Biosci. **180**, 29–48 (2002).

26. Van den Driessche, P. & Watmough, J. Further notes on the basic reproduction number. Math. Epidemiol. Lect. Notes Math. **1945**, 159–178, DOI: 10.1007/978-3-540-78911-6_6 (2008).

27. Chai, W. K. & Pavlou, G. Path-based epidemic spreading in networks. IEEE/ACM Trans. Netw. **25**, 565 – 578 (2017).

28. Van Mieghem, P., Omic, J. & Kooij, R. Virus spread in networks. IEEE/ACM Trans. Netw. **17** (2009).

29. Van Mieghem, P. The n-intertwined sis epidemic network model. Computing **93**, 147–169 (2011).

30. Van Mieghem, P. Performance analysis of Complex networks and systems (Cambridge University Press, 2014).

31. Achterberg, M. A. & Van Mieghem, P. Moment closure approximations of susceptible-infected-susceptible epidemics on adaptive networks. Phys Rev E **106** (2022).

32. Anderson, R. M. & May, R. M. Infectious Diseases of Humans (Oxford University Press, 1991).

33. Diekmann, O., Heesterbeek, J. & Roberts, M. The construction of next-generation matrices for compartmental epidemic models. J R Soc Interface **7(47)**, 873–85, DOI: 10.1098/rsif.2009.0386 (2010).

34. Ganesh, A., Massoulié, L. & Towsley, D. he effect of network topology on the spread of epidemics. IEEE 24th Annu. Jt. Conf. IEEE Comput. Commun. Soc. 1455–1466 (2005).

35. Wang, Y., Chakrabarti, D., Wang, C. & Faloutsos, C. Epidemic spreading in real networks: an eigenvalue viewpoint. $22^n d$ Int'l. Symp. Reliab. Distributed Syst. (SRDS) 25–34 (2003).

36. Chakrabarti, D., Wang, Y., Wang, C., Leskovec, J. & Faloutsos, C. Epidemic thresholds in real networks. ACM Trans. Inf. Syst. Secur. **10**, 1–26 (2008).

37. Guo, D., Trajanovski, S., Van de Bovenkamp, R., Wang, H. & Van Mieghem, P. Epidemic threshold and topological structure of susceptible-infectious-susceptible epidemics in adaptive networks. Phys Rev E **88** (2013).

38. Erdős, P. & Rényi, A. On random graphs i. Publ. Math. **6**, 290–297 (1959).

39. Barabasi, A. L. & Albert, R. Emergence of scaling in random networks. Science **286(5439)**, 509–512 (1999).

Author contributions statement

W.K.C conceived the model and experiments. Both authors performed the model development, result analysis and writing of the manuscript.

Data Availability

Data generated during the current study are available from the corresponding author on reasonable request.

Additional information

The authors declare no competing interests.